LANGMUIR

pubs.acs.org/Langmuir Article

# Effect of Oil Properties on the Generation of Nano-Aerosols During Bubble Bursting Through Crude Oil−Dispersant Slicks

Diego F. Muriel, Subhamoy Gupta, and Joseph Katz*

Cite This: *Langmuir* 2021, 37, 13365−13378 Read Online

ACCESS | Metrics & More | Article Recommendations | Supporting Information

**ABSTRACT:** This study examines the effect of dispersant and oil properties on the aerosolization of fresh and weathered surface crude oil slicks by bursting of a plume of ∼0.7 mm bubbles. A scanning mobility particle sizer measures the size distribution of aerosols in the 20−400 nm range in a clean air chamber. The 500-$\mu$m-thick slicks contain oils with varying origin, viscosity, interfacial tension, and weathering state. Test are performed with and without premixed dispersant (Corexit 9500A), which reduces the oil−seawater interfacial tension by 2 orders of magnitude at a dispersant-to-oil ratio (DOR) of 1:25. When compared to aerosolization in clean seawater, the nano-aerosol concentration decreases for slicks without dispersant but increases by 27%−351% upon introduction of dispersant. For most cases, the airborne nanodroplet concentration increases with decreasing Capillary or Morton numbers as well as the ratio of the so-called inner to thermal length scales. To explain the airborne nanodroplet generation in an oil−dispersant mixture, we show that prior to bubble injection, even minimal agitation of the interface causes generation of a subsurface cloud of nanodroplets that diffuses away from the interface. This process appears to be caused by thermal capillary instability when the interfacial tension is low enough to increase the thermal length scale to a few nanometers.

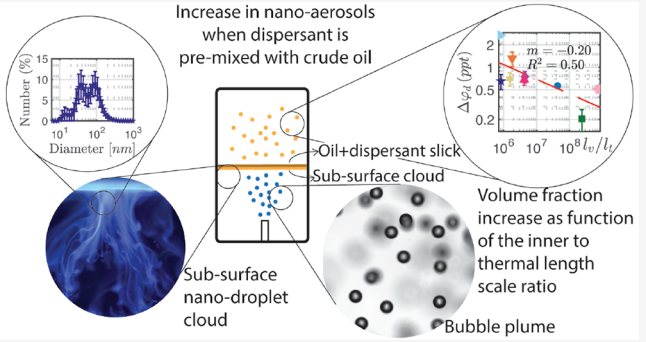


## 1. INTRODUCTION

Oil spills of the magnitude of the Deepwater Horizon spill[1] are rare, but their environmental impact is extensive, lasting decades.[2,3] As the spilled oil can persist beyond a decade in toxic forms and quantities, it might compromise the health, growth, and reproduction of species; impacts that go beyond the acute-phase mortality.[4] Furthermore, if the oil reaches beaches or marshes, harmful contamination affecting local fauna might persist for decades.[5] Smaller spills are more common than large events, often resulting from operations in oil and port terminals.[6] Despite their limited scale, their environmental impact is significant.[7] Application of dispersant is one of the few available remediation techniques intended to reduce the environmental impacts of spills. Dispersants are water- and oil-soluble surfactants that reduce the oil−water interfacial tension.[8] Consequently, they enhance breakup of oil into small droplets, thereby accelerating their transport in the water column.[9,10] The environmental impact of releasing dispersants into the ocean has been a subject for considerable debate.[8,11−13] Application of dispersant on the ocean surface raises also questions about its impact on aerosolization of oil and entrainment of volatile organic compounds (VOC) into the atmosphere. Aerosol are likely to survive for days in the lower atmosphere and can be carried downwind by the atmospheric boundary layer.[14] There are several sources of aerosol associated with a spill, including secondary organic aerosols originating from the evaporating hydrocarbons, soot created by in situ burning, and droplets generated as surface waves interacting with slicks. The latter can produce airborne particles either by splashing associated with breaking waves or by bubble bursting.[15] As the breaking waves entrain air into the water column, the bubbles rise back to the surface and burst in a process involving several types of marine aerosol generation mechanisms, e.g. film droplets and jet droplets.[16−21] Film drops are generated when the thin film between the bubble and the surface shatters and the receding rims break up into small droplets. The jet droplets are generated as the bubble cavity collapses and shoots up a central jet that breaks up into several droplets.[15] During the Deepwater Horizon spill, 7 million L of dispersants, including Corexit 9500A and 9527A, were sprayed on the surface and injected into the oil plume.[3] The organic aerosols were dispersed in a wide plume and had a measurable effect on ambient levels of aerosol in coastal communities directly downwind.[14]

**Received:** August 1, 2021
**Revised:** October 22, 2021
**Published:** November 5, 2021






https://doi.org/10.1021/acs.langmuir.1c02047
*Langmuir* 2021, 37, 13365−13378

The effect of dispersant on aerosol production by breaking waves and bubble bursting in oil-contaminated seawater has been previously demonstrated for Louisiana crude oil. Ehrenhauser et al.[22] investigated the simultaneous subsurface injection of oil and bubbles into a seawater column and provided data for the total airborne particulate matter above the surface. They showed that bursting of 550 to 870 $\mu$m bubbles caused emission of organic particles and that premixing the oil with dispersant increased their total mass. Afshar-Mohajer et al.[23] studied the particulate and gaseous emissions from crude oil and crude oil−dispersant surface slicks due to plunging breaking waves. For a dispersant to oil ratio (DOR) of 1:25, they found that the total number of submicron airborne particles is 1−2 orders of magnitude higher than those of pure crude oil slicks for sizes ranging between 10 and 400 nm. In contrast, the dispersant causes a reduction in the VOC concentration, consistent with previous field data[24,25] and simulations.[26] Sampath et al.[27] investigated the aerosol production by a bubble bursting through the slicks of crude oil and DOR 1:25 oil−dispersant mixtures. They concluded that for bubbles larger than ∼600 $\mu$m diameter (referred to as "large bubbles"), the dispersant increases the concentration of airborne nanoparticles by at least 1 order of magnitude. Associated chemical analysis confirmed the presence of airborne oil above the slicks. In contrast, bubbles in the 86−178 $\mu$m range did not have a significant impact on the nano-aerosols. Hence, they concluded that the dispersant-induced nanodroplet generation is associated with formation of film droplets. Afshar-Mohajer et al.[28] used the above-mentioned breaking wave data[23] to assess the health risks caused by the detected VOC and particulates. They concluded that the use of dispersant reduces the benzene cancer risks, yet the noncarcinogenic hazard quotients associated with the lower VOC still raise exposure concerns. However, the higher nanoparticle concentration increases the total mass burden to the human respiratory system by about ten times. Finally, Afshar-Mohajer et al.[29] measured the effect of dispersant on the oil mass fraction in the airborne particles using the same setup as in the work of Sampath et al.[27] For DOR of 1:25, the aerosolized oil masses are 2.37 and 5.82 higher than those of cases without dispersant for aerodynamic diameters of airborne particulate matter smaller than 2.5 $\mu$m ($PM_{2.5}$) and 220 nm, respectively. They are interested in $PM_{2.5}$ because more than 55% of these particles tend to deposit in the alveolar region of the human respiratory system[30] and interact with the lungs.[31] As for the ultrafine particles, i.e. those with diameters smaller than 100 nm, they are associated with a variety of pulmonary diseases, upper respiratory tract irritation,[32−34] and disruption of systemic vascular function.[35,36] Considering that crude oil composition and properties vary substantially, it would be of interest to determine how the dispersant affects the concentration of nano-aerosols in other crude oils. Furthermore, prior studies showed that the efficacy of dispersant decreases as the oil undergoes a weathering process.[37] Hence, it would be of interest to determine how early stages of weathering, which involves evaporation of the light oil components,[38] affects the generation of nano-aerosols.

The objective of this study is to determine the effect of dispersant on the generation of nano-aerosols as bubbles burst in slicks of crude oils with varying properties, including origin, viscosity, density, and interfacial tension, and undergoing early phases of weathering. The results enable us to determine the relationship between these properties and nanodroplet concentration in the 20−400 nm range. As noted above, droplets of this size range are of particular interest owing to their interaction with human respiratory system and health concerns. The experimental setup and instrumentation are described in the next section. The results presented in the following chapter show that dispersant causes an increase in the nano-aerosol concentration for all the tested fresh and partially weathered oils. Expressing the observed trends in terms of dimensionless parameters derived from the oil properties allows us to generalize the findings. For the most part, the nanodroplets volume fractions increase with decreasing Capillary and Morton numbers, and the ratio of "inner" to thermal length scales. To elucidate the origin of the nanodroplets, in the Discussion section, auxiliary experiments demonstrate that they are generated initially below the surface owing to thermal capillary instabilities.

## 2. MATERIALS AND METHODS

**2.1. Exposure Chamber and Bubble Generation.** The measurements were performed in a sealed 0.7 m high and 0.3 × 0.3 $m^2$ cross section acrylic tank, which is illustrated in Figure 1a. The

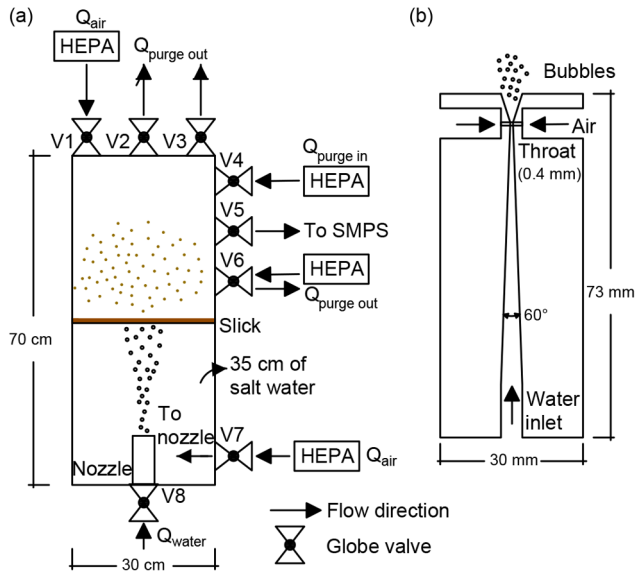


**Figure 1.** Aerosolization chamber (a) and bubble generation nozzle (b).

0.35 m liquid column contained artificial seawater (Instant Ocean) with a salinity of 33 parts per thousand and the density, viscosity, and surface tension listed in Tables 1 and 2. The bubble plume was generated by injecting pressurized seawater with the same properties through a custom-made nozzle illustrated in Figure 1b at a prescribed volumetric flow rate ($Q_w$). HEPA-filtered air was introduced at a controlled volumetric flow rate ($Q_a$) from two radially opposite, 0.4 mm diameter ports located in the 0.4 mm throat of the nozzle. The water sheared the injected air to generate a bubble plume, similar to approaches used in prior studies.[39−41] The characteristic bubble size was adjusted by varying $Q_a/Q_w$. In the present study both were kept constant, with $Q_a$ = 20.0 ± 0.5 $cm^3$/min and $Q_w$ = 10.2 ± 0.7 $cm^3$/min, resulting in a plume containing bubble sizes large enough to produce the elevated nano-aerosols, as described by Sampath et al.[27] The injection of water and bubbles into the tank increased the water level in the tank by 7.5 mm after 66 min (total injection time), corresponding to a change of 3.2% in the bubble rise distance and 2.1% reduction in the air volume. Allowing an outflow to compensate for this change might have introduced undesired secondary flows, which would have affected the bubble plume and caused oil or


https://doi.org/10.1021/acs.langmuir.1c02047
Langmuir 2021, 37, 13365−13378

**Table 1. Sea Water, Dispersant, Oil, and Oil−Dispersant Mixture Properties: Viscosity and Density at 20.50 and 25.00 °C**

| | fresh and weathered oils | | | | fresh and weathered oil-dispersant mixture | | | |
|---|---|---|---|---|---|---|---|---|
| | 20.50 ± 0.02 °C | 20.5 ± 0.2 °C | 25.00 ± 0.02 °C | 25.0 ± 0.2 °C | 20.50 ± 0.02 °C | 20.5 ± 0.2 °C | 25.00 ± 0.02 °C | 25.0 ± 0.2 °C |
| | viscosity (mPa s) | density (kg/m$^3$) | viscosity (mPa s) | density (kg/m$^3$) | viscosity (mPa s) | density (kg/m$^3$) | viscosity (mPa s) | density (kg/m$^3$) |
| Sea water | 1.06 ± 0.01 | 1061.2 ± 3.6 | 0.95 ± 0.01 | 1046.4 ± 3.6 | N/A | N/A | N/A | N/A |
| Dispersant | 56.65 ± 0.25 | 983.8 ± 9.1 | 45.32 ± 0.30 | 977.7 ± 3.3 | N/A | N/A | N/A | N/A |
| Bakken | 8.40 ± 0.03 | 874.8 ± 6.2 | 7.05 ± 0.04 | 873.2 ± 8.3 | 9.00 ± 0.04 | 887.0 ± 2.0 | 7.25 ± 0.09 | 873.0 ± 5.4 |
| Louisiana | 9.63 ± 0.13 | 872.7 ± 3.3 | 8.24 ± 0.54 | 870.5 ± 4.7 | 12.34 ± 0.55 | 888.8 ± 7.1 | 8.69 ± 0.19 | 873.6 ± 3.0 |
| Hoops | 9.69 ± 0.21 | 879.3 ± 4.7 | 9.01 ± 0.34 | 878.8 ± 4.7 | 11.67 ± 0.11 | 904.3 ± 3.7 | 8.67 ± 0.25 | 878.8 ± 8.1 |
| ANS | 33.61 ± 0.39 | 924.9 ± 2.3 | 26.37 ± 0.23 | 922.8 ± 4.3 | 36.09 ± 0.13 | 925.3 ± 4.0 | 25.12 ± 0.40 | 907.0 ± 6.5 |
| P. Henry | 218.1 ± 4.1 | 948.2 ± 6.4 | 151.0 ± 3.8 | 944.0 ± 3.7 | 199.15 ± 4.8 | 967.5 ± 3.4 | 151.8 ± 3.2 | 939.8 ± 5.8 |
| Cold Lake | 362.0 ± 7.2 | 963.8 ± 8.9 | 277.9 ± 6.3 | 949.8 ± 3.7 | 374.2 ± 4.8 | 984.8 ± 6.1 | 278.8 ± 4.6 | 947.8 ± 8.3 |
| Louisiana weathered | 25.66 ± 0.50 | 903.3 ± 8.5 | 14.49 ± 0.24 | 902.5 ± 3.3 | 22.06 ± 0.35 | 905.2 ± 1.7 | 16.06 ± 0.20 | 888.3 ± 2.9 |
| Hoops weathered | 26.59 ± 0.31 | 905.7 ± 6.4 | 14.74 ± 0.11 | 903.0 ± 4.8 | 25.54 ± 0.24 | 925.8 ± 5.5 | 17.88 ± 0.20 | 894.7 ± 2.6 |
| ANS weathered | 111.5 ± 0.6 | 945.7 ± 4.2 | 47.82 ± 0.58 | 943.8 ± 11.2 | 93.40 ± 0.30 | 937.8 ± 5.7 | 60.00 ± 2.43 | 925.7 ± 9.8 |

**Table 2. Sea Water, Dispersant, Oil, and Oil−Dispersant Mixture Properties: Surface Tension and Oil−Water Interfacial Tension**

| | fresh and weathered oils | | | | fresh and weathered oil-dispersant mixture | | | |
|---|---|---|---|---|---|---|---|---|
| | temp[a] ± 0.1 | surface tension with air (mN/m) | temp[a] ± 0.1 | interfacial tension with seawater (mN/m) | temp[a] ± 0.1 | surface tension with air (mN/m) | temp[a] ± 0.1 | interfacial tension with seawater (mN/m) |
| Sea water | 20.1 | 74.65 ± 0.29 | N/A | N/A | N/A | N/A | N/A | N/A |
| Dispersant | 18.8 | 26.28 ± 0.29 | N/A | N/A | N/A | N/A | N/A | N/A |
| Bakken | 19.9 | 27.54 ± 0.23 | 19.6 | 5.19 ± 0.13 | 19.7 | 27.80 ± 0.13 | 18.8 | 0.11 ± 0.01 |
| Louisiana | 19.4 | 27.33 ± 0.04 | 19.0 | 21.55 ± 0.35 | 19.7 | 27.95 ± 0.32 | 18.8 | 0.35 ± 0.01 |
| Hoops | 19.9 | 25.20 ± 0.72 | 18.3 | 9.51 ± 0.22 | 19.4 | 28.01 ± 0.18 | 18.8 | 0.12 ± 0.01 |
| ANS | 19.2 | 28.81 ± 0.76 | 17.8 | 9.67 ± 0.31 | 19.4 | 28.64 ± 0.39 | 18.8 | 1.05 ± 0.04 |
| P. Henry | 19.5 | 28.15 ± 0.96 | 18.3 | 26.95 ± 0.13 | 18.7 | 30.57 ± 0.06 | 18.8 | 0.99 ± 0.01 |
| Cold Lake | 20.8 | 30.36 ± 0.31 | 17.8 | 19.66 ± 0.17 | 18.7 | 31.58 ± 0.86 | 18.8 | 3.28 ± 0.19 |
| Louisiana weathered | 19.8 | 28.86 ± 0.07 | 17.8 | 17.8 ± 0.11 | 18.8 | 28.98 ± 0.13 | 18.8 | 1.24 ± 0.01 |
| Hoops weathered | 19.8 | 28.08 ± 0.10 | 18.3 | 7.21 ± 0.31 | 18.8 | 29.35 ± 0.07 | 19.2 | 0.29 ± 0.01 |
| ANS weathered | 19.8 | 29.79 ± 0.52 | 18.3 | 9.63 ± 0.19 | 18.8 | 30.13 ± 0.10 | 19.4 | 1.15 ± 0.01 |

[a]Measured at room temperature.

dispersants transport out of the tank. Therefore, we opted to let the surface level rise slowly and did not allow any outflow of water during the experiments.

Back illuminated imaging using a halogen lamp through a diffusion paper was used to measure the bubble size distributions. The 11.49 mm × 11.49 mm sample area was located 10.2 mm below the still water surface, and data were recorded at two depths, one matching the center of the tank and the other 5 mm away from it. Statistically independent samples that did not contain the same bubbles were acquired by recording 2000 images at 2 frames per second using a 2016 pixel × 2016 pixel CMOS camera (PCO dimax) equipped with a 200 mm Nikkor lens. A machine learning-based pixelwise classification procedure, consisting of the following steps, was implemented to determine the bubble diameters. First, using the downloadable software package Ilastik,[42] semantic segmentation was used for classifying parts of the images as background and foreground (i.e., bubbles). The training features included descriptors of pixel intensity, edge sharpness involving a series of filters (Laplacian of Gaussian, Gaussian gradient magnitude, difference of Gaussians) and texture (structure tensor eigenvalues, Hessian of Gaussian eigenvalues). The training was performed for 10 different kernel sizes, corresponding to bubble diameters. The random forest, consisting of 100 decision trees and 2 features per node, was trained for each image based on manually labeled training sets. The result of this step was a map of the probability that a certain pixel belongs to the background or foreground. Second, using the ImageJ package,[43] instance segmentation aimed at defining the bubbles starting with global thresholding based on the Otsu's method,[44] followed by distance transform watershed to separate overlapping bubbles, and culminating with measurement of the bubble size. The bubble number density distribution (see Figure S1 in the Supporting Information) was unimodal, with a mean diameter and standard deviation of $\overline{d_b} = 730.2 \pm 34.1$ $\mu$m, implying that the bubble generation rate was about 98 000 bubbles per minute. Furthermore, following the work of Zhang et al. and Sampath et al.,[27,45] planar fluorescence imaging was used to corroborate the bubble statistics. The seawater was mixed with trace amounts of fluorescent dye (Rhodamine WT) and illuminated with a 3 mm thick laser sheet to create a bright background, which illuminated the bubbles passing through. Reflection of the surrounding fluorescence from the bubble surface, generated rings defining the boundaries of the bubbles. The measured mean bubble diameter was 4.5% (32.6 $\mu$m) smaller than that determined from the machine learning procedures.

**2.2. Oil Properties.** The present study involved a series of oils with varying properties, including Bakken,[46] Louisiana sweet (MCR252),[3,47,48] Hoops,[49] Alaskan North Slope (ANS),[46,50] Cold



https://doi.org/10.1021/acs.langmuir.1c02047
Langmuir 2021, 37, 13365−13378

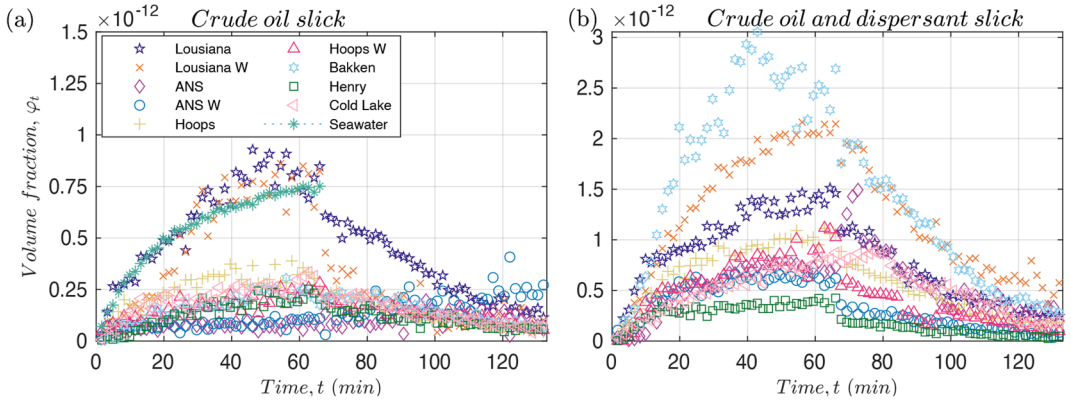


**Figure 2.** Aerosol production as a function of time, $\varphi_t$: (a) aerosol volume fraction for seawater and slick cases and (b) for slick with premixed dispersant cases.

Lake,[46] and Platform Henry,[51] as listed in Table 1. Bakken, Louisiana, ANS, and Platform Henry are crude oils, Cold Lake is a diluted bitumen,[46] and Hoops is a blend of five constituent fields.[49] These oils were either "freshly drawn" from the barrels or "weathered" by evaporating 10% of their weights by aeration and subsequently tested. For the weathering process, compressed air was introduced through a diffusion stone at 9.5 L/min, and the weight of the crude oils was monitored until the desired evaporation percentage was achieved.[52−55] Each fresh and weathered oil was tested with and without premixed Corexit 9500A (Nalco Environmental Solutions LLC) dispersant at a dispersant to oil ratio (DOR) of 1:25. The primary components of Corexit 9500A are 18% by weight ionic surfactant DOSS (dioctyl sodium sulfosuccinate), 27% nonionic surfactants, including Span 80, Tween 80, and Tween 85, and 55% carrier solvents, including dipropylene glycol butyl ether and petroleum distillates.[56]

The viscosities of the fresh crude oil, weathered oil, and oil−dispersant mixtures were measured in an MCR302 Anton Paar rheometer equipped with a 50 mm diameter cone−plate. Each test was performed while increasing the shear rate from 1 to 100 1/s and decreasing the duration from 10 to 1 s, both linearly. One hundred data points were collected consecutively during each test, and six independent tests were performed for each oil and oil−dispersant mixture. Some of the oils, typically the lighter ones, exhibited Newtonian behavior, i.e. their viscosity did not vary with shear rate. For a few of the cases, typically the heavier oils (Henry, Cold Lake, ANS), Newtonian behavior persisted up to shear rates of 70−80 1/s and then started decreasing at higher levels. The data presented in Table 1 corresponds to least-squares fitting of the data in the Newtonian range. All the viscosity measurements were performed at 20.5 and 25 °C and subsequently linearly interpolated for each case according to the room temperature during the experiments. The viscosity of the salt water was determined with a Cannon−Frenske viscometer. The oil density was measured by weighing a known volume. The uncertainties in viscosity and density reported on Table 1 represent the 95% confidence interval estimated from a Bayesian bootstrap analysis involving 10 000 randomly selected subsets from all the measurements, assuming a *t*-distribution.[57−59] The surface tension in air and the oil−saltwater interfacial tension were measured using the pendant drop method.[60,61] The uncertainty reported in Table 2 also represents the 95% confidence interval obtained from a Bayesian bootstrap analysis; this time based on 30 independent test. The pendant drop method was not suitable for measuring the interfacial tension of the DOR 1:25 oils owing to difficulties in maintaining a stable pendant droplet when the interfacial tension decreased to very low levels. Hence, the interfacial tension of oil−dispersant mixtures was calculated from the oblateness of submillimeter (0.37−0.98 mm diameter) droplets rising in a 1.2 m quiescent seawater column, following recipes provided in the work of Bozzano et al.[50] and Hu et al.[62,63] Images of the rising droplet were captured at 1200 Hz using a 2016 pixel × 2016 pixel CMOS camera (PCO dimax) at a spatial resolution of ∼3.6 μm/pixel (3.1× magnification). Between 61 and 900 images per test were converted to binary masks by global thresholding based on Otsu's method.[44] The centroid, minor, and major axes of the droplet images where determined based on a regional analysis of the binary image using available Matlab routines. Between 5 and 11 independent tests were performed for each case, and the uncertainty was based on a bootstrap analysis. As shown in Table 2, while the surface tension was not modified significantly by the addition of dispersant, the interfacial tension was reduced by 1 to 2 orders of magnitude, depending on the crude oil.

**2.3. Measurement of Nano-Aerosols.** The size and concentration of nanosized particles, in the 20.2−399.5 nm range, were measured using a scanning mobility particle sizer spectrometer (SMPS) model 3938 (TSI Inc.), equipped with an advanced aerosol neutralizer (model 3088, TSI Inc.), an electrostatic classifier model 3082, and a condensation particle counter (CPC) model 3787. The airborne particulate matter was scanned every 99 s, including 6 and 3 s for equipment retracing and purging, respectively. In the SMPS spectrometer system, the electrostatic classifier sorted particles based on their electrical mobility and the CPC counted them.[64] An impactor with an orifice diameter of 0.071 cm installed at the inlet to the SMPS removed particles larger than 0.956 μm at the selected flow rate of 0.60 ± 0.09 L/min based on information provided by TSI. This impactor and flow rate provided a higher cutoff diameter than that reported in the work of Sampath et al.[27] Each base case, i.e., bubbling through clean seawater without slick, and slick case were repeated three times. The base case consisted of 60 min of air purging after filling with clean seawater, followed by 40 scans prior and 40 scans during bubble bursting, each lasting 99 s, for a total time of 132 min. For each experiment involving a slick, with or without dispersant, the acquisition sequence consisted of 60 min of air purging after the slicks had been created, and 40 scans prior, 40 scans during, and 40 scans after bubble bursting, for a total time of 198 min. The volume required to form a 500-μm thick slick over the entire surface was poured gently and distributed as uniformly as possible over the surface. Once bubbling started, all slicks appeared to be uniformly distributed. The temperature, pressure, and relative humidity of the sampled air was measured inside the electrostatic classifier of the SMPS. They varied between 17.25 and 22.52 °C, 99.85 and 101.1 KPa, and 63.3 and 88.3%, respectively (see Figures S2−S4 in the Supporting Information).

The number size distributions presented in this paper show the measured values without accounting for effects of relative humidity on the particle diameter, i.e., not the dry particle diameters. Hysteresis effects and dry particle diameters involving salt water droplets, which are a strong function of relative humidity, could be estimated using the particle growth factor reported in the work Zieger et al.[65] Based on this paper, the hygroscopic growth factor of submicron sea-salt droplets at the experimental relative humidity ranges between 1.5 and


https://doi.org/10.1021/acs.langmuir.1c02047
Langmuir 2021, 37, 13365−13378

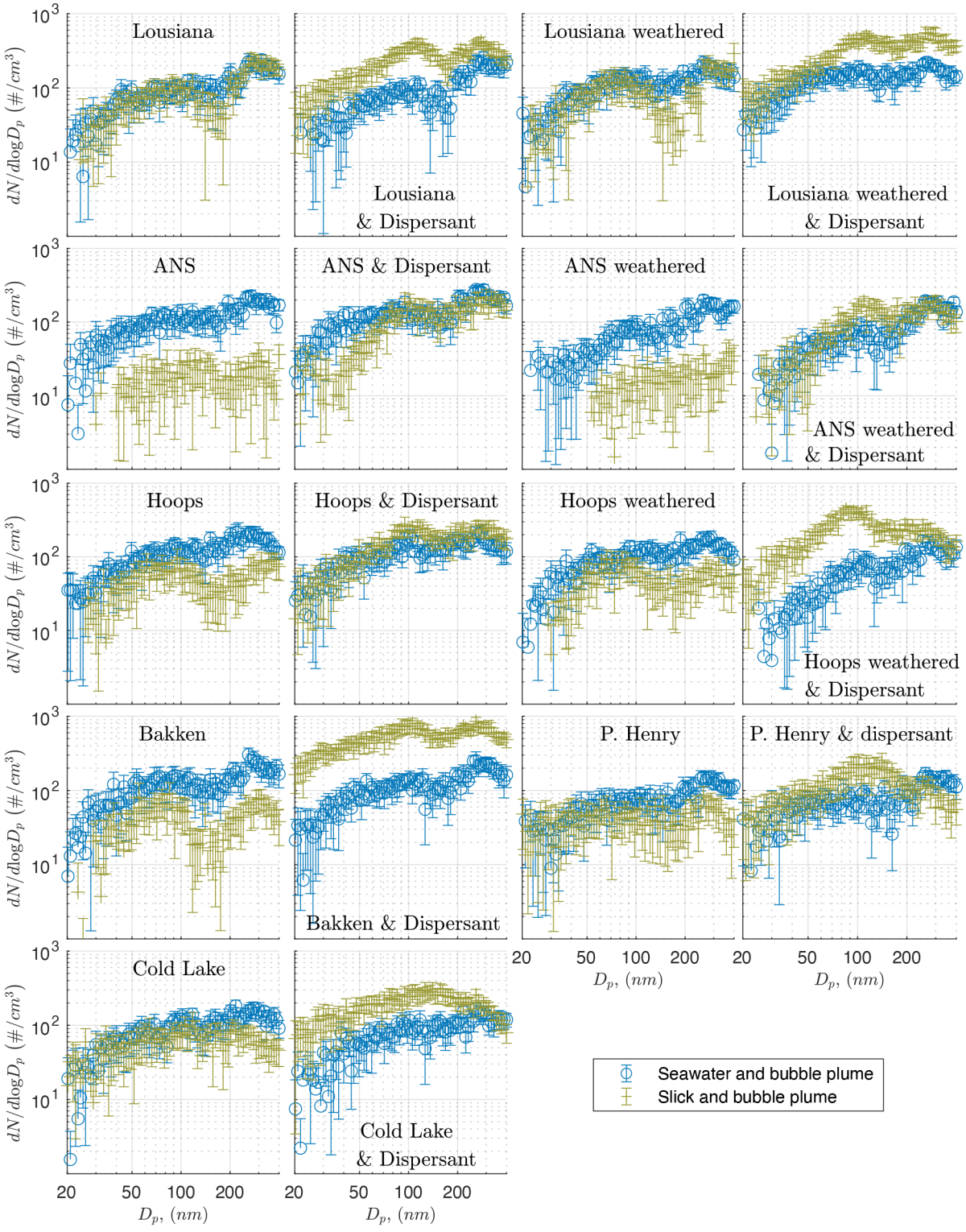


**Figure 3.** Aerosol production for oil and oil with premixed dispersant slicks compared to baseline (i.e., clean seawater under the action of a bubble plume).

2.2. Therefore, the dry particle diameters can be approximated by dividing the presented values by 1.5−2.2. For droplets/particles that contain both salt and oil or for ambient particles, however, the relevant growth factor is expected to be lower. As a reference, Afshar-Mohajer et al.[29] show that 32.6% and 8.8% of the aerosols mass for Louisiana oil slicks is oil for cases with no dispersant and DOR 1:25, respectively. However, the total mass of airborne oil is 2.4 times higher with dispersant owing to differences in the total mass of the aerosol. The chamber's purging and cleaning protocols are described in the Appendix.

**2.4. Data Processing.** For each case (base case and slicks), the first scan after purging have not been used; hence only 39 scans were used for the baseline measurements prior to bubble busting. The three repetitions are concatenated, resulting in 117, 120, and 120 scans


https://doi.org/10.1021/acs.langmuir.1c02047
Langmuir 2021, 37, 13365−13378